CHEMISTRY OF MATERIALS

pubs.acs.org/cm

Article

Enlightening the Well-Controlled Photochemical Behavior of 1,1-Dicyanomethylene-3-Indanone-Functionalized π-Conjugated Molecules

Parag Das, Cory T. Kornman, Ion Ghiviriga, Khalil A. Abboud, and Ronald K. Castellano*

Cite This: *Chem. Mater.* 2023, 35, 8122–8134

Read Online

ACCESS | Metrics & More | Article Recommendations | Supporting Information

ABSTRACT: 1,1-Dicyanomethylene-3-indanone (INCN) is a popular electron acceptor showcased in hundreds of push−pull oligomers, including some of the best nonfullerene acceptor (NFA) materials used in small molecule-based bulk-heterojunction (BHJ) organic photovoltaics (OPVs). Consequences of the configuration (i.e., *Z* or *E*) and conformation (i.e., s-*cis* or s-*trans*) of the exocyclic olefin that conjugates INCN to π-conjugated molecules have largely been ignored. Two recent reports have implicated *Z*/*E* photoisomerization in the photodegradation of popular NFAs like IT-4F when subjected to broad spectrum irradiation. Here, we elucidate through experiments and complementary ground- and excited-state computations the photochemical behavior of a family of eight INCN-functionalized donor−acceptor molecules varying in aryl and heteroaryl substitution, alkyl group substitution, and halogen functionalization on the INCN unit. Well-controlled *Z*/*E* photoisomerization using selective wavelengths of excitation spanning the ultraviolet and visible regions is observed in all cases yielding a range of *Z*/*E* photostationary state (PSS) distributions with no evidence of a previously reported photooxidation. *Z*/*E* photoisomerization followed by sequential pericyclic reactions, consistent with one recent literature report, is identified for just one target molecule upon irradiation at 454 nm. The alkyl group positioning on the thiophene ring neighboring the INCN is found to bias the conformational preferences of the target molecules and modulate access to this reaction pathway. All eight molecules undergo facile *Z*/*E* photoswitching over numerous cycles upon selective excitation. Overall, the work reveals the well-controlled photochemical behavior of INCN-functionalized π-systems and encourages their use in the design of future functional and organic materials and photoswitches.

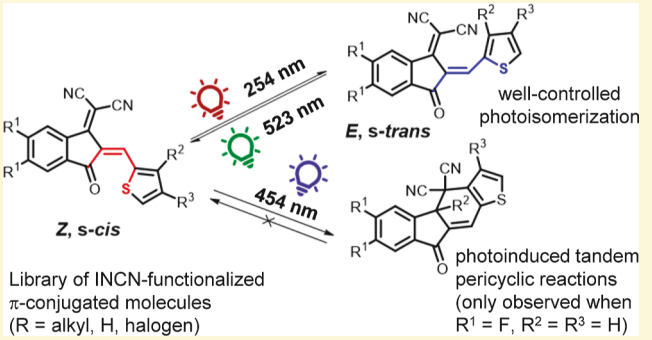

Downloaded via UNIV OF FLORIDA on December 21, 2023 at 15:02:17 (UTC).
See https://pubs.acs.org/sharingguidelines for options on how to legitimately share published articles.

INTRODUCTION

1,1-Dicyanomethylene-3-indanone (INCN, Figure 1a)[1,2] was introduced in 2015 as an electron-deficient structural unit within an acceptor−donor−acceptor (A−D−A) type π-conjugated oligomer ITIC (Figure 1b),[3−5] one of the best nonfullerene acceptors (NFAs) for organic photovoltaic (OPV) applications reported until that time.[3] NFAs quickly received attention given their potential to overcome shortcomings associated with fullerene-based electron acceptors such as poor molecular HOMO−LUMO gap tunability and weak absorption in the visible spectral region.[6−8] NFAs functionalized with the INCN unit have since become mainstays within the OPV community due to strong and broad absorption in the visible to near-infrared (NIR) region and high electron mobilities that are a consequence of favorable π-stacking and good crystallinity.[9−12] Indeed, the 2015 debut article featuring the INCN acceptor has received 3200+ citations, speaking to the important role that this structure has played in the development of OPV materials.[3] To date, advancements in INCN-containing NFAs have ushered in additional record-breaking power conversion efficiencies (PCEs), surpassing 18% for single-junction OPV devices.[12−15]

It is well-appreciated that small changes in NFA structure can alter the morphology of the organic solar cell active layer and affect overall device efficiency.[16] Common molecular-level approaches to optimizing OPV thin film morphology and charge transport[17−19] include modifying the π-conjugated backbone structure and/or planarity and the structure and/or placement of solubilizing side chains.[20−24] Modifications specific to INCN-containing molecules include altering the solubilizing alkyl chain placement along the π-conjugated backbone[25] or on the indanone ring[26] and introduction of halogen atoms[27] or methoxy groups[28] to various positions. The

Received: June 26, 2023
Revised: September 6, 2023
Published: September 21, 2023

© 2023 American Chemical Society

https://doi.org/10.1021/acs.chemmater.3c01607
Chem. Mater. 2023, 35, 8122−8134

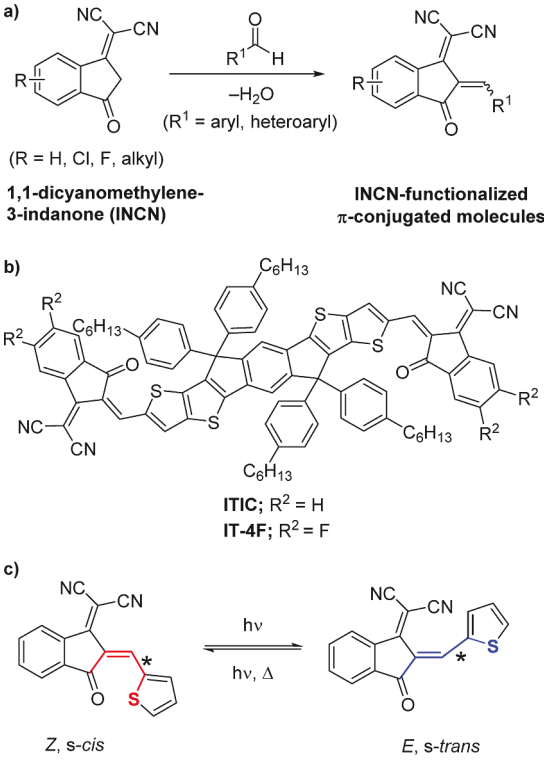

Figure 1. (a) The 1,1-dicyanomethylene-3-indanone (INCN) acceptor unit and the standard Knoevenagel approach to its installation. (b) Structure of nonfullerene acceptors (NFAs) ITIC and IT-4F. (c) Parent INCN-functionalized thiophene depicted in the *Z* configuration (red) and the *E* configuration (blue). The conformation about the bond indicated with an asterisk (*) is shown as s-*cis* and s-*trans*, respectively, with respect to the sulfur atom of the thiophene ring.

structural changes, while sometimes seemingly minor, can induce a higher film absorption coefficient, larger crystalline coherence, and higher electron mobility, ultimately leading to higher PCE.

We recently reported the ability of dicyanorhodanine (RCN) functionalized thiophenes to undergo *Z*/*E* configurational isomerization upon photoirradiation[29] and observed that the solid-state morphologies and optoelectronic properties of thin films from RCN-containing oligomers can be significantly affected by configurational composition.[24] Our structure–property studies could encourage opportunities for solar cell optimization through the consideration of this stereochemical feature. In the same spirit, it is surprising that the structural and functional consequences of *Z*/*E* stereoisomerism with respect to the exocyclic double bond that links INCN to a π-conjugated moiety have generally been overlooked (Figure 1c). In fact, there are instances where molecules featuring INCN have been depicted in the peer-reviewed literature with arbitrary configurations (*Z* or *E*) and conformations (s-*cis* or s-*trans*), with no experimental justification.[30−32] Likewise, with the exception of only a few reports,[33−35] limited attention has been given to the photochemistry of the conjugated INCN structure despite its analogy to systems with olefins that participate in well-controlled photoisomerization reactions that are the basis for photoswitch development.[36−38]

Two recent and notable literature reports have appeared on INCN-related photochemistry, as it specifically relates to the stability of IT-4F and its congeners. One, a combined experimental and theoretical study by Perepichka et al., examines how A−D−A molecules containing the INCN unit can be susceptible to photodegradation upon irradiation and implicates *Z*/*E* photoisomerization as a critical mechanistic step (Figure 2a).[33] The authors specifically consider the

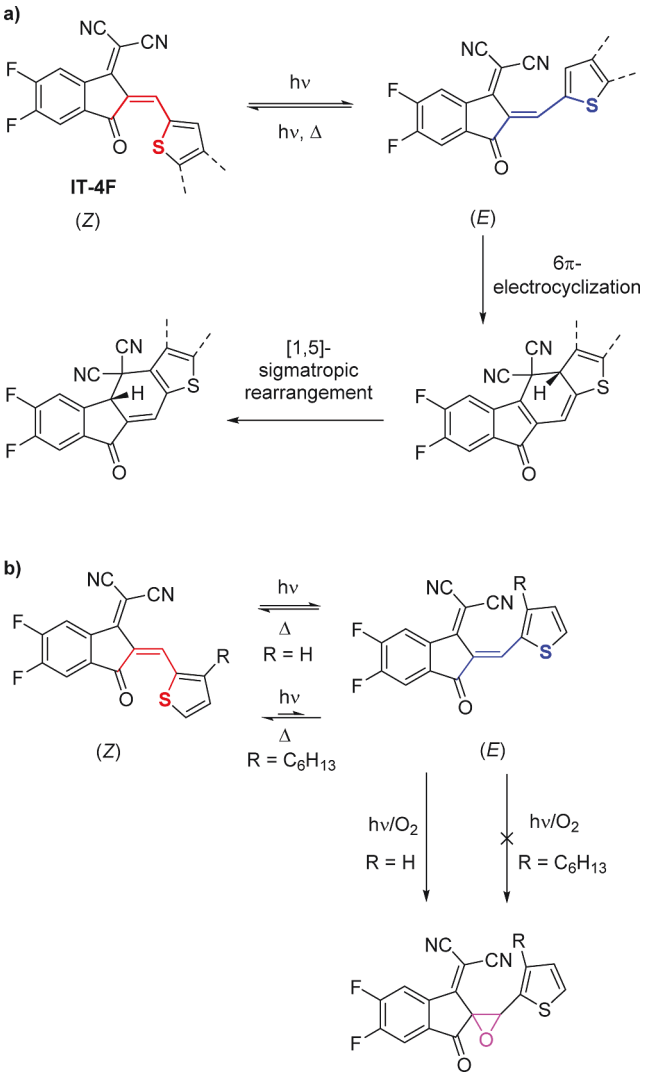

Figure 2. (a) Mechanism of photodegradation of IT-4F proposed by Perepichka and co-workers[33] involving double bond isomerization of the INCN acceptor unit from the *Z* isomer (red) to the *E* isomer (blue), followed by tandem electrocyclization/sigmatropic rearrangement. (b) Consecutive photoisomerization and photooxidation behavior of difluorinated INCN reported by Li and co-workers.[34]

response of IT-4F to broad wavelength irradiation (400−2500 nm, λ_{max} = 1100 nm, 250 W quartz halogen lamp).[33,39] The product of the photodegradation reaction results from *Z*/*E* isomerization about the terminal INCN moiety, followed by a tandem 6π−electrocyclization reaction and 1,5-hydride shift that restores aromaticity to the adjacent thiophene unit (Figure 2a). In a separate report, Li and co-workers show the ability of difluorinated INCN compounds including IT-4F to undergo *Z*/*E* photoisomerization under one-sun-equivalent illumination provided by a metal halide lamp similar to the work by Perepichka and co-workers,[33] but claim a subsequent photoepoxidation reaction as their end fate (Figure 2b).[34] The authors additionally find that the photoepoxidation is suppressed by installing an alkyl chain on the adjacent thiophene

https://doi.org/10.1021/acs.chemmater.3c01607
Chem. Mater. 2023, 35, 8122−8134

(Figure 2b), supporting a volume-conserving isomerization hypothesis. Discrepancies among these two reports (e.g., tandem electrocyclization/sigmatropic rearrangement vs epoxidation using similar broad-wavelength irradiation sources) and our observations of well-controlled, wavelength-dependent photoisomerization using selective irradiation sources for related RCN-based systems[29] prompted our current deeper dive into the photochemical behavior of INCN π-systems.

Herein, we report the photochemical behavior of a family of eight INCN-functionalized donor−acceptor molecules varying in aryl and heteroaryl substitution, alkyl group substitution, and halogen functionalization on the INCN unit (**1***Z*−**8***Z*, Figure 3). Photoirradiation experiments were performed using

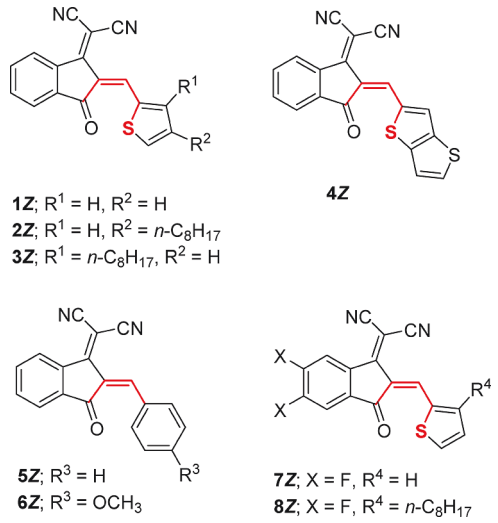

Figure 3. Chemical structures of INCN compounds **1**−**8** studied in this work. The molecules are shown in the *Z* configuration and the *s-cis* conformation (if relevant).

different wavelengths of excitation (λ_{irr}) spanning the ultraviolet and visible regions (λ_{irr} = 254, 371, 454, and 523 nm). Well-controlled *Z*/*E* photoisomerization reactions yielding varying compositions of *Z* and *E* isomeric mixtures at the photostationary state (PSS) are observed in all cases. The photooxidation behavior as mentioned in the work by Li and co-workers[34] is not observed for any of the studied molecules upon selective irradiation. However, *Z*/*E* photoisomerization followed by tandem pericyclic reactions, consistent with the work of Perepichka and co-workers,[33] is identified *for just one target molecule*, **7**, and *only upon selective irradiation at 454 nm*. Additionally, alkyl group positioning on the thiophene ring neighboring the INCN is found to bias the conformational preference of the target molecules and modulate access to the pericyclic reaction pathway. All target molecules are shown to undergo facile *Z*/*E* photoswitching over numerous cycles upon selective excitation. The experimental results are confirmed by complementary ground- and excited-state (TD-DFT) density functional theory (DFT) calculations that allow the photochemical behavior to be understood based on molecular geometry/conformation and ground state energy differences that accompany structural changes at the acceptor and donor units. Overall, the work unveils how INCN-functionalized π-systems show well-controlled photochemistry and behave analogously to established small molecule photoswitches including azobenzenes, stilbenes, hemithioindigos, diarylethenes, and dicyanorhodanines,[29,37,40−42] and encourages their usage in the design of future functional organic materials.

RESULTS AND DISCUSSION

Design and Synthesis. Compound **1***Z* serves as the simplest INCN-functionalized π-conjugated thiophene analogue and a benchmark. Considering the role of the alkyl solubilizing chain on the photodegradation behavior of INCN-functionalized NFAs discussed in the literature (vide supra),[33,34] compounds **2***Z* and **3***Z* introduce an octyl chain in positions 4 and 3 of the thiophene, respectively. Compound **4***Z* with its thieno[3,2-*b*]thiophene substituent mimics the structural features present in common NFA molecules, such as ITIC and IT-4F. Compounds **5***Z* and **6***Z* evaluate benzene and *p*-methoxybenzene, common aromatic substituents in related molecular photoswitches, on the INCN photochemical behavior. Finally, targets **7***Z* and **8***Z* are inspired by the literature (vide supra),[34] where only the former was shown to undergo photoepoxidation.

Full synthetic schemes and details for target molecules **1***Z*−**8***Z* and intermediates are provided in the Supporting Information (Schemes S1−S3, pages S3−S10). Using the preparation of **1***Z* as an example (Scheme 1), the parent INCN

Scheme 1. Synthesis of Model Compound 1*Z*

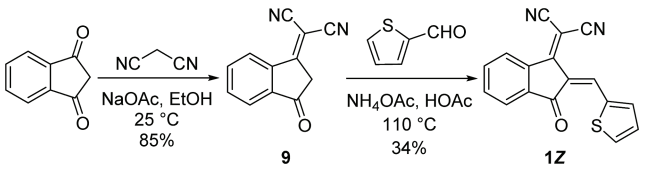

acceptor unit (compound **9**) is accessed through a condensation of 1,3-indanedione and malononitrile, followed by a Knoevenagel condensation with the appropriate formylated aryl/heteroaryl unit. In all cases, the *Z* isomer is obtained as the only detectable isomer from the synthesis. Worth noting here, although the *Z* and *E* isomers display slightly different R_f values by thin-layer chromatography (TLC) on silica gel, the isomers coeluted regardless of eluent composition and we were unable to isolate pure samples of the *E* isomers for independent studies.

Stereochemical Determination. The stereochemistry of the exocyclic double bond of as-synthesized **1** was determined from a single crystal X-ray structure (Figure 4a). The ORTEP representation of **1** shows the monomer in the *Z* configuration, with a unit cell containing four molecules of **1***Z* (Figure 4c). The long-range herringbone packing of **1***Z* displays a slip-stack arrangement and a $\pi-\pi$ stacking distance of 3.35 Å as measured between planes defined by neighboring thiophenes (Figures 4b and S51). A slightly twisted geometry is adopted by **1***Z* in the crystal, presumably to suppress a steric interaction between the $C(CN)_2$ substituent and the adjacent olefin proton. The twisting causes a small deviation from planarity between the isomerizable (C8−C12) double bond and the INCN carbocycle, defined by a C7−C8−C12−C13 dihedral angle of −1.71° (Figure 4a). An intramolecular distance of 2.73 Å between the carbonyl oxygen and thiophene sulfur atom is consistent with chalcogen bonding (e.g., S···O interactions) identified in previously reported structures.[43,44]

Since we were unable to isolate a pure sample of **1***E*, we modeled the *Z* and *E* forms of compound **1** in the gas-phase

https://doi.org/10.1021/acs.chemmater.3c01607
Chem. Mater. 2023, 35, 8122−8134

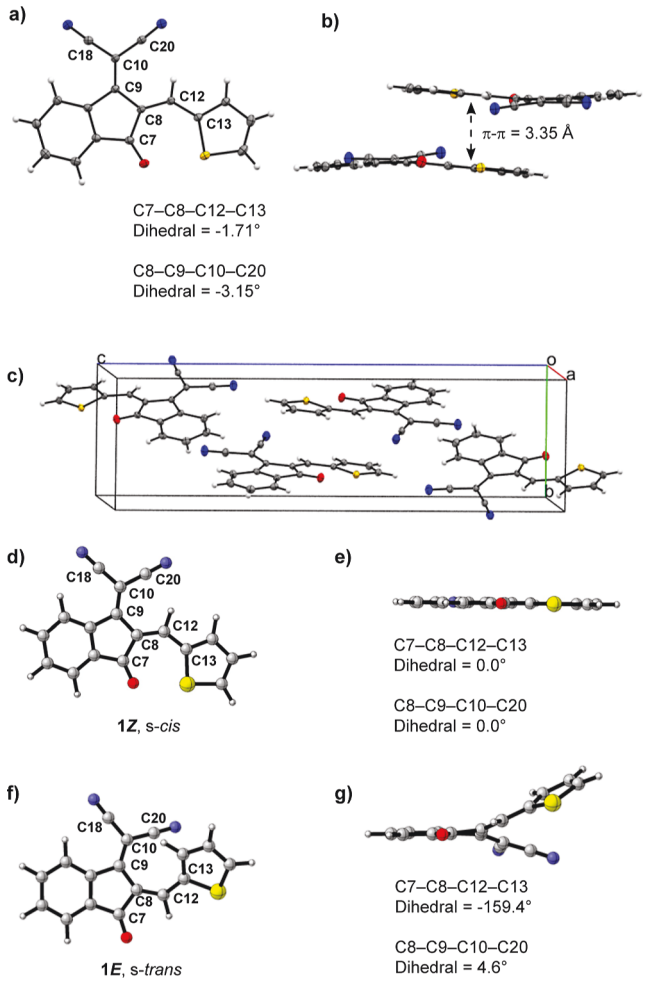

Figure 4. Single crystal X-ray and computed structures of **1**. (a) ORTEP representation of the **1***Z* monomer (thermal ellipsoids are set at a 50% probability level), (b) stacking between two molecules of **1***Z* in the solid state, and (c) unit cell containing four molecules of **1***Z*. Optimized, lowest energy conformers [DFT, B3LYP/6-31+G(d)] of (d) **1***Z* (face-on view), (e) **1***Z* (edge-on view), (f) **1***E* (face-on view), and (g) **1***E* (edge-on view).

(DFT, B3LYP/6-31+G(d), Figure 4d–g). Though the X-ray crystal structure of **1***Z* reveals a slightly twisted form, DFT predicts a planar geometry (Figure 4d,e) for **1***Z*. Interestingly, the **1***E* isomer appears to be highly twisted. Here, a C7–C8–C12–C13 dihedral angle of −159.4° represents a 20.6° deviation from planarity due to steric repulsion between the $C(CN)_2$ group and the adjacent thiophene (Figure 4f,g). The dicyano moiety in **1***E* is also twisted, with C8–C9–C10–C18 and C8–C9–C10–C20 dihedral angles of 178.6 and 4.6°, respectively (Figure 4f). Additional computational results are discussed below.

The stereochemistries of **1***Z* and **1***E* were also determined in solution using 2D NMR methods. IPAP-gHSMBC (15 mM, chloroform-*d*) analysis of a **1***Z*/**1***E* mixture obtained via irradiation to the photostationary state (PSS) using 254 nm light (Figure 5, vide infra) shows that the three-bond heteronuclear coupling constant ($^{1,3}J_{CH}$) between the isomerizable olefin proton (H12) and the INCN carbonyl carbon (C7) is much larger for the *Z* isomer ($^{1,3}J_{C7-H12}$ = 9.1 Hz) than for the *E* isomer ($^{1,3}J_{C7-H12}$ = 5.2 Hz, Figure S6). On the other hand, the $^{1,3}J_{CH}$ coupling between the INCN vinyl carbon (C9) and exocyclic olefin proton (H12) is much smaller for the *Z* isomer ($^{1,3}J_{C7-H12}$ = 4.8 Hz) compared to the *E* isomer ($^{1,3}J_{C7-H12}$ = 9.8 Hz, Figure S6), agreeing well with literature precedent from similar systems.[29,43] Furthermore, HSQC and HMBC experiments allowed complete chemical shift assignments for **1***Z* and **1***E* (Figures S1–S5) and reveal that the olefin proton of **1***Z* is significantly deshielded (δ = 8.95 ppm) relative to the same proton in **1***E* (δ = 8.13 ppm). The deshielding arises from the proximity of the olefin proton in **1***Z* to the dicyanomethylene group, is universally observed for INCN-functionalized target molecules (**1**–**8**), and allows for convenient stereochemical determination by routine 1D ^{1}H NMR experiments.

NMR Photoisomerization Studies. The well-controlled photoisomerization reactions of **1***Z*–**8***Z* could be conveniently monitored by ^{1}H NMR by comparing the spectra of the as-synthesized isomers (*Z* form) to the spectra of the irradiated samples. All of the studies were performed using aerated solutions of compounds **1***Z*–**8***Z*. Full details of the irradiation sources used for photoisomerization experiments can be found in the Supporting Information (Figure S7, pages S33–S34). For compound **1**, clean *Z* → *E* photoisomerization is observed upon selective irradiation at 254 nm and the reaction can be monitored by ^{1}H NMR to evaluate the extent of isomerization (15 mM, chloroform-*d*). Within 15 min of irradiation, the as-synthesized isomer (**1***Z*) converts photochemically into the metastable form (**1***E*) to yield an inseparable **1***Z*/**1***E* mixture. The new ^{1}H NMR signals correspond to the metastable **1***E* form (Figure 5, top spectrum), with no evidence of pericyclic reaction products or photooxidation products. When compound **1***Z* is irradiated until no further changes in the ^{1}H NMR integral ratios are observed, the photostationary state (PSS) is achieved with an isomeric ratio of 51% **1***Z* and 49% **1***E*. The results suggest well-controlled photoisomerization of **1** under 254 nm irradiation conditions in chloroform (Figure 5). Although silica gel TLC analysis of the **1***Z*/**1***E* mixture obtained postirradiation (λ_{irr} = 254 nm) shows a very minor difference in R_f value between the two isomers (Figure S8a), with the *E* isomer appearing slightly more polar than the *Z* form, the *E* isomers could not be separated from the *Z*/*E* mixture using column chromatography for any of the model compounds due to overlap between the *Z* and *E* isomers (Figure S8b).

Encouraged by the photoisomerization behavior of **1** with 254 nm irradiation, we investigated other wavelengths to assess any wavelength dependence on the observed photochemical behavior. A range of **1***Z*/**1***E* mixtures were obtained at the PSS upon exposure of **1***Z* to 371, 454, and 523 nm light in solution (Table 1, Figure 6). Well-behaved photoisomerization (*Z* → *E*) was observed with 254, 371, and 523 nm excitation (Figure 6), while minor degradation was observed with 454 nm irradiation along with formation of the typical **1***Z*/**1***E* mixture (Figure 6, blue spectrum). The degradation behavior observed with 454 nm irradiation may be due to formation of other photogenerated species that could not be characterized. A concentration-dependent study in solution (chloroform-*d*) was also performed for compound **1**, revealing no influence of concentration on the observed PSS isomeric ratios within a concentration range of 5–20 mM (Figure S9). The result suggests no significant intermolecular noncovalent interactions in solution within this concentration range. Photoisomerization studies of model compounds **2***Z*–**6***Z* in solution (15 mM, chloroform-*d*) also reveal well-controlled isomerization behav-

https://doi.org/10.1021/acs.chemmater.3c01607
Chem. Mater. 2023, 35, 8122–8134

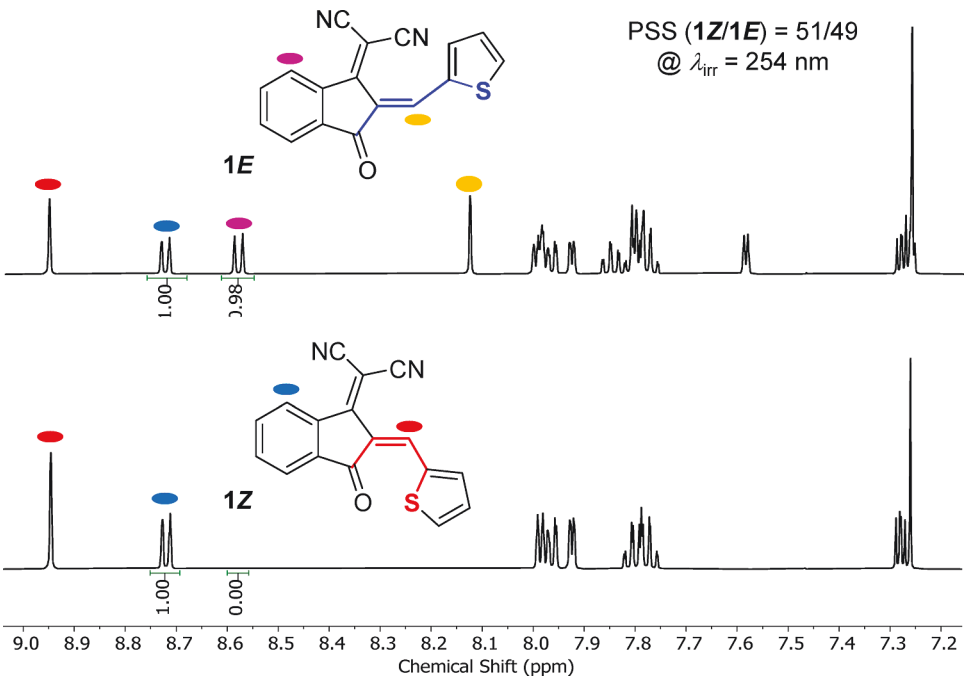

Figure 5. ^{1}H NMR spectra (15 mM, chloroform-*d*) of pure **1***Z* (bottom) and a 51/49 **1***Z*/**1***E* mixture (top) obtained after irradiation to a photostationary state using 254 nm light. No evidence of pericyclic reactions or photooxidation was observed for **1** under these irradiation conditions.

Table 1. *Z*/*E* Isomeric Compositions at the Photostationary State (PSS) Observed in Solution for Target Molecules 1−8 Upon Selective Excitation at Different Wavelengths

irradiation wavelength (nm)	*Z*/*E* composition (%/%) at the PSS for **1**−**8**[a]							
	1	**2**	**3**	**4**	**5**	**6**	**7**	**8**
254	51/49	54/46	57/43	61/39	39/61	48/52	46/54	64/36
371	45/55	49/51	48/52	53/47	48/52	50/50	42/58	52/48
454	40/60[b]	39/61[b]	35/65	37/63[b]	40/60[b]	42/58[b]	41/59[c]	41/59
523	80/20	77/23	74/26	69/31	43/57	63/37	78/22	76/24

[a]For each sample, the PSS ratios have been reported based on three measurements (with an error of ±1%). [b]Minor degradation observed. [c]Tandem pericyclic reactions observed.

ior using different irradiation sources, yielding a range of *Z*/*E* mixtures at the PSS (Table 1). However, compounds **2**, **4**, **5**, and **6** show minor evidence of photodegradation upon 454 nm irradiation, similar to compound **1** (Table 1, Figures S10−S14).

While INCN-based π-conjugated molecules were reported to undergo photoepoxidation at the exocyclic double bond under one-sun-equivalent illumination at ambient conditions,[34] we were unable to verify this behavior for compounds **1**−**6** using selective excitation (λ_{irr} = 254, 371, 454, 523 nm, chloroform-*d*). To further investigate the photooxidation behavior, we were interested in analyzing the isomerization of previously reported compound **7** using selective excitation sources instead of one-sun-equivalent illumination.[34] Upon selective irradiation of **7** at 254, 371, and 523 nm in solution (15 mM, chloroform-*d*), well-controlled photoisomerization was observed yielding a range of 7*Z*/7*E* mixtures at the PSS (Table 1, Figure S15), with no evidence of other photochemical products. Interestingly, irradiation at 454 nm results in the typical 7*Z*/7*E* (41/59) mixture along with generation of new signals visible in the postirradiation ^{1}H NMR spectrum (Figure 7), indicating the formation of the sigmatropic rearrangement product (Figure S16).

After prolonged irradiation (24 h) of **7** with 454 nm light, signals corresponding to 7*Z* and 7*E* diminished, and the resultant mixture was purified using silica column chromatography to obtain compound **15** (Figure 7), the formation of which is consistent with *Z*/*E* photoisomerization followed by photoinduced tandem pericyclic reactions (Scheme 2). A six electron electrocyclic reaction can take place from photogenerated 7*E* resulting in the electrocyclization product (compound **16**, Scheme 2), followed by a 1,5-hydride shift to form the sigmatropic rearrangement product (compound **15**, Scheme 2). The results observed for compound **7** upon 454 nm irradiation agree well with the results first presented by Che et al. for IT-4F under metal-halide lamp irradiation.[33] Interestingly, molecule **1** was not susceptible to pericyclic reactions even upon prolonged irradiation with 454 nm light, instead showing only minor evidence of photodegradation, while the PSS composition of **1***Z*/**1***E* (40/60) remains unaltered after prolonged 454 nm irradiation (Figure 6, Table 1).

The ground state energies of the intermediates involved in the photoisomerization followed by tandem pericyclic reactions have been calculated using DFT to better understand the difference in the photochemical outcomes of compounds **1**

https://doi.org/10.1021/acs.chemmater.3c01607
Chem. Mater. 2023, 35, 8122−8134

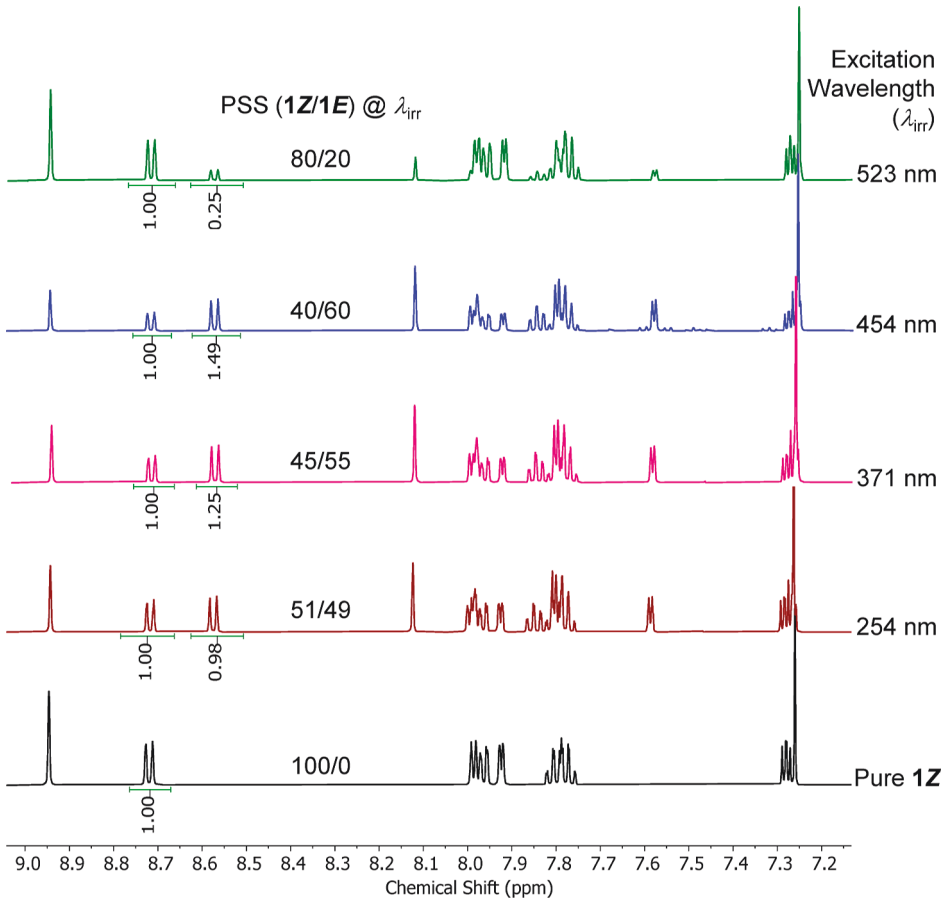

Figure 6. ^{1}H NMR spectra (15 mM, chloroform-*d*) showing pure **1***Z* (bottom, black spectrum) and **1***Z*/**1***E* mixtures obtained after 254 nm irradiation (maroon spectrum), 371 nm irradiation (pink spectrum), and 523 nm irradiation (green spectrum) in chloroform-*d*. No evidence of pericyclic reactions or photooxidation were observed for **1** under these irradiation conditions.

and **7** based on atomic substitutions (Scheme 2). The calculations reveal a lower energy for the electrocyclized intermediate for fluorine substituted **16** compared to hydrogen substituted **18** (Scheme 2). The difference in relative energy between the lowest energy conformer of 7*E* and intermediate **16** (13.6 kcal/mol) is much less than that between the lowest energy conformer of **1***E* and **18** (15.8 kcal/mol). Moreover, the final rearranged product **15** is found to be 1.42 kcal/mol *more stable* than 7*Z*, while product **17** is 1.18 kcal/mol less stable than **1***Z*, suggesting a more favorable tandem pericyclic reaction pathway for compound **7**. Interestingly, molecules **3** and **8** show only well-behaved photoisomerization under all irradiation conditions (Table 1, Figures S11, S17) which must be due to a steric influence provided by the alkyl chain on carbon 3 of the thiophene (vide infra).

UV−Vis Photoisomerization Studies. To study the different photochemical behaviors in more depth, we also performed photoirradiation studies of the aerated solutions of model compounds **1***Z*−**8***Z* using UV−vis spectroscopy. The primary and secondary absorption bands of **1***Z* in solution (20 μM, chloroform) lie at 438 and 330 nm, respectively, and can be classified as $\pi \rightarrow \pi^*$ transitions (Figure S25). The time-dependent density functional theory (TD-DFT) calculations were conducted using a range-separated hybrid functional (CAM-B3LYP) and double-ζ basis set (cc-pVDZ) that has been proven adequate for similar push−pull systems.[46,47] The TD-DFT predicted absorption profiles show similar trends compared to the UV−vis profiles, where the primary and secondary absorption bands lie at 375 and 291 nm, respectively (Figure S25). The primary band can also be attributed to a HOMO−LUMO transition, as confirmed by inspection of the frontier molecular orbitals through DFT simulations (Table S1 and Figure S38). The secondary absorption band corresponds to multiple transitions including HOMO − 4−LUMO + 1 (Table S1 and Figure S38). Conducting similar photoirradiation experiments using UV−vis, for compound **1**, well-controlled photoisomerization is observed upon irradiation at 254 nm. A gradual decrease in the absorbance of the primary band is observed with further irradiation time along with a gradual increase in absorbance of the secondary band, until the PSS is reached, where no changes in absorbance are observed (Figure 8a). As pure **1***E* could not be isolated, the UV−vis spectra of **1***Z* and **1***E* were simulated using time-dependent (TD-DFT) calculations to gain insight into how the olefin stereochemistry of INCN-functionalized compounds influences the optical and electronic properties of the systems (Figures 8b and S25). In general, the simulated UV−vis spectra for **1***Z* and **1***E* predict that the *Z* and *E* isomers display very similar absorption profiles with significant spectral overlap in both primary and secondary absorption bands. A 13 nm red shift is observed for **1***E* (λ_{max} = 389 nm) at the primary absorption band compared to that for **1***Z* (λ_{max} = 376 nm). To be noted, a significant decrease in the molar absorptivity at the primary absorption band and a notable increase at the secondary one are observed for **1***E* (Figure 8b, dashed blue line) by TD-DFT calculations, as compared to **1***Z* (Figure 8b,

https://doi.org/10.1021/acs.chemmater.3c01607
Chem. Mater. 2023, 35, 8122−8134

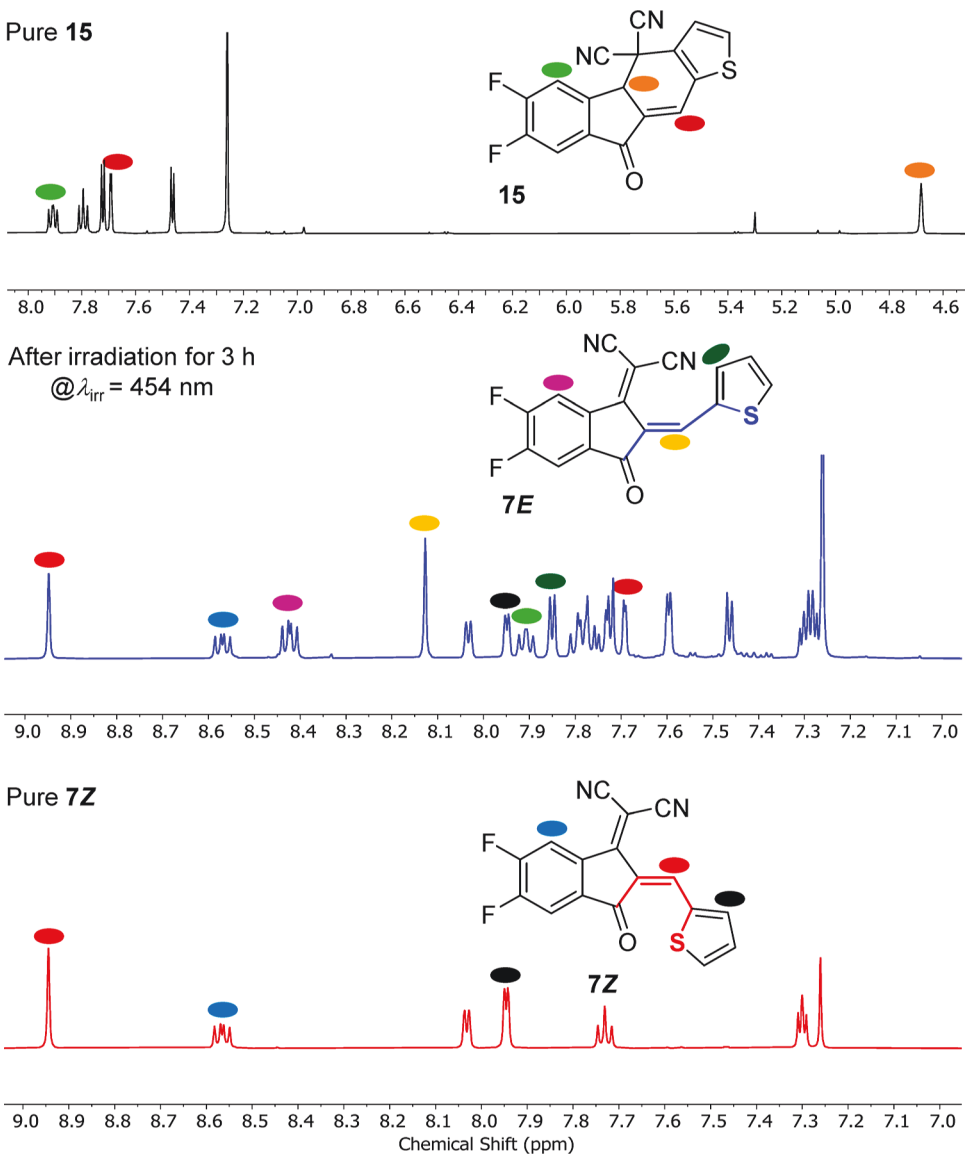

Figure 7. ^{1}H NMR spectra (15 mM, chloroform-*d*) showing pure 7*Z* (bottom, red spectrum), a mixture of 7*Z*, 7*E*, and **15** (middle, blue spectrum) after 3 h of irradiation at 454 nm, and purified compound **15** (top, black spectrum), achieved after prolonged 454 nm irradiation of 7*Z* and chromatographic purification of the mixture.

dashed red line), which is very similar to what is observed in solution. Furthermore, when pure **1***Z* is irradiated with 454 and 523 nm light sources, a very similar absorbance trend is observed. The normalized absorbance plot of **1** in solution (Figure 8b, solid line) suggests that the highest decrease in absorbance of the primary absorption band is observed upon 454 nm irradiation, followed by 254 and 523 nm, indicating the extent of photoisomerization at different irradiation wavelengths. The trend in the **1***Z*/**1***E* distributions in solution at the PSS using different irradiation sources shows a strong correlation between the NMR and UV−vis data.

The UV−vis spectroscopy data for **2**−**8** also correlate well with the NMR results. The absorption maxima in solution (20 μM, chloroform) of all of the model compounds are summarized in Table 2. The normalized absorption spectra (Figures S26−S33) of the compounds in solution show that the primary absorption bands lie in the visible region, whereas the secondary bands are observed in the UV region. For compounds **2**−**6** and **8**, upon irradiation at 254, 454, and 523 nm, a significant decrease in absorbance is observed at the primary absorption band, whereas there is little change observed at the secondary absorption band. All compounds have shown well-behaved photoisomerization upon selective irradiation. However, for some compounds, a decrease in the secondary absorption band is observed at the PSS using 454 nm light, which might correspond to the minor degradation observed by ^{1}H NMR analysis (Figures S10−S17). Time-dependent DFT calculations of the *Z* and *E* isomers also predict two absorption bands for these model compounds (Table 2). The simulated normalized absorption spectra (Figures S25−S33) suggest that the molar absorptivity at the primary absorption band of the *E* isomer is lower than that of the *Z* form. The trend observed in the solution absorption profiles of the compounds match quite well with the simulated ones. UV−vis spectroscopy in solution (20 μM, chloroform) also confirms the different photochemical behaviors of molecule 7*Z* using selective irradiation sources. Upon irradiation with 254 and 523 nm light, compound **7** shows

https://doi.org/10.1021/acs.chemmater.3c01607
Chem. Mater. 2023, 35, 8122−8134

Scheme 2. Mechanism of Tandem *Z*/*E* Isomerization, Electrocyclization, and Sigmatropic Rearrangement for Compounds 1 and 7[a]

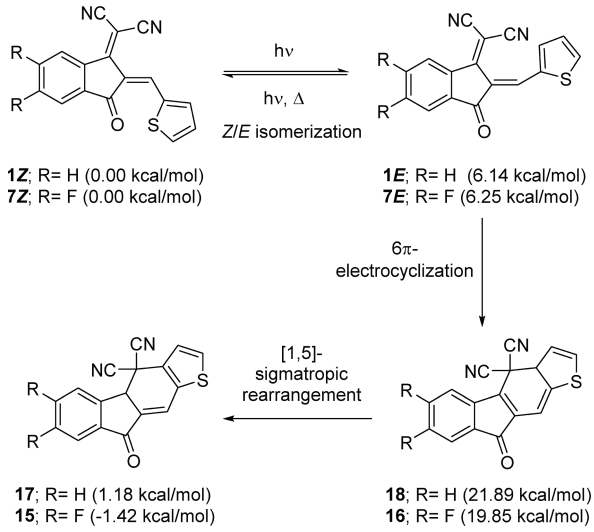

[a]The relative energies of all the intermediates involved in the tandem reactions are denoted in parentheses [based on DFT calculations performed in the gas-phase at the B3LYP/6-31+G(d) level of theory].

well-behaved photoisomerization (Figure 9a). A decrease in absorbance is observed at the primary absorption band, whereas a small increase is found at the secondary absorption band, as predicted by time-dependent DFT calculations for 7*Z* and 7*E*. However, upon prolonged irradiation with 454 nm light, a gradual decrease in absorbance at both the primary and secondary absorption bands is observed (Figure 9b).

Upon prolonged irradiation with 454 nm light, an absorption maximum in the UV−vis profile is observed at 241 nm, along with secondary absorption bands at 372 and 499 nm (Figure 9b, blue trace). The absorption band lying at 372 nm might demonstrate the formation of compound **15** as the absorption maximum coincides with that of purified **15** in solution (λ_{max} = 365 nm, Figure 9b, purple trace). The absorption profile of **15** can also be predicted by time-dependent DFT calculations, which match quite well with the solution results (Figures 9b, S32). The absorption bands at 241 and 499 nm, observed upon prolonged irradiation in solution, might be attributed to the formation of **16**, as the absorption bands (234 and 496 nm) obtained from the time-dependent DFT calculation of **16** coincide well with the experimental ones (Figure 9b).

UV−Vis Photoswitching Studies. We studied the reversibility of the photoisomerization reactions by performing photoswitching studies. All of these experiments were performed using aerated solutions of the model compounds. Irradiating molecule **1** in solution (20 μM, chloroform) with a shorter wavelength (λ_{irr} = 454 nm) light source promotes $Z \rightarrow E$ isomerization to obtain a PSS and exposing the PSS mixture to a longer wavelength of irradiation (λ_{irr} = 523 nm) promotes $E \rightarrow Z$ isomerization until a new PSS is reached (Figure 10a). Interestingly, even after ten photoswitching cycles, the system appears highly fatigue resistant, and the photoswitching is facile. We also performed similar photoswitching experiments with other target molecules, differing in end group substitution (**3** and **8**), conjugation length (**4**), donor unit structure (**6**), and substitution at the INCN unit (**7** and **8**). Molecule **3**

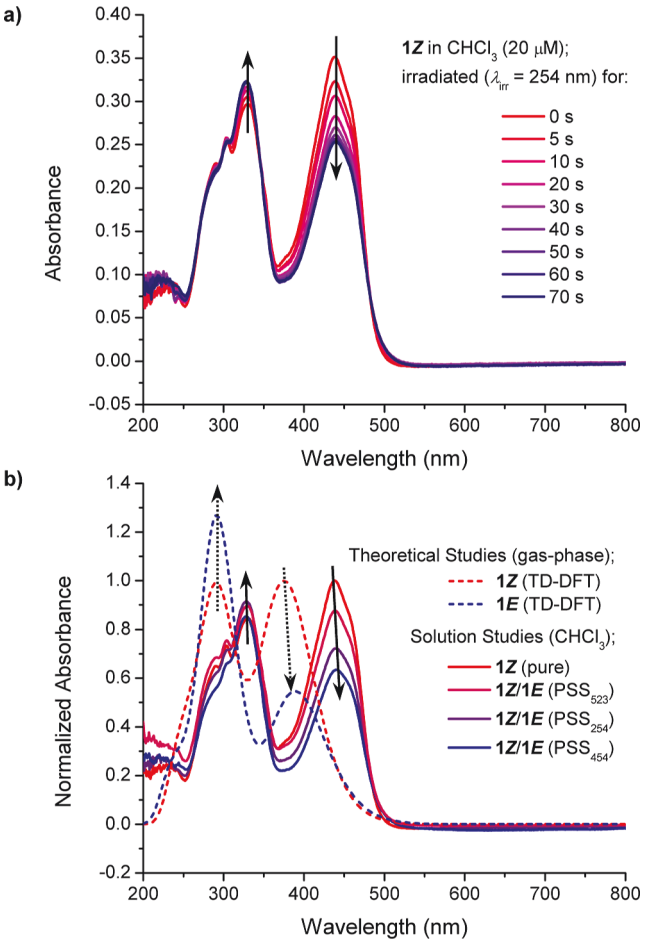

Figure 8. (a) Overlayed absorption spectra of **1** in solution upon irradiation using 254 nm light. (b) Normalized absorption spectra in solution (solid line) of pure **1***Z* (red) and upon irradiation with different light sources (λ_{irr} = 254, 454, and 523 nm) at the PSS in solution and time-dependent DFT predicted UV−vis spectra (dashed line) of **1***Z* (red) and **1***E* (blue).

(Figure S34), **4** (Figure S35), **6** (Figure S36), and **8** (Figure S37) undergo facile photoswitching and are highly fatigue resistant upon exposure to alternating irradiation sources between 454 and 523 nm over numerous cycles. Photoswitching of compound **7** was performed using alternating irradiation sources of 254 and 523 nm over ten irradiation cycles (Figure 10b). Molecule **7** undergoes facile photoswitching, with a minor decrease in maximum absorbance values over ten cycles. The photoswitching results for compound **7** demonstrate the importance of excitation wavelength in the observed photochemistry of INCN-functionalized molecules, with no evidence of either electrocyclization reactions or photooxidation reactions after numerous cycles of alternation between 254 and 523 nm light (Figure 10b). This photostability encourages structural or electronic engineering of INCN derivatives to address the currently large overlap in primary and secondary absorption bands, which should, in turn, allow tuning the PSS isomeric ratios and exploration of stimuli-responsive materials.

Ground State DFT Studies. We have shown well-controlled photoisomerization in solution of a series of INCN-functionalized donor−acceptor molecules upon selective irradiation with no evidence of photoepoxidation. While a photoinduced pericyclic reaction pathway was observed for **7**,

https://doi.org/10.1021/acs.chemmater.3c01607
Chem. Mater. 2023, 35, 8122−8134

Table 2. DFT Simulated and Solution Absorption Studies of the Model Compounds

model compounds	gas phase DFT studies					solution studies in chloroform	
	relative energy of *E* isomer[a] (kcal/mol)	absorption maximum (nm)				absorption maximum of *Z* isomer (nm)	
		primary band		secondary band			
		Z isomer	*E* isomer	*Z* isomer	*E* isomer	primary band	secondary band
1	6.14	376	389	291	291	439	330
2	5.75	381	397	293	293	453	334
3	5.23	385	402	297	297	454	337
4	6.25	408	421	305	305	496	363
5	3.09	352	356	288	283	385	317
6	3.73	377	397	296	294	449	336
7	6.25	376	392	292	292	442	323
8	5.37	386	406	297	297	475	336

[a]Energy values reported of the most stable conformer in the *E* form relative to that in the *Z* form.

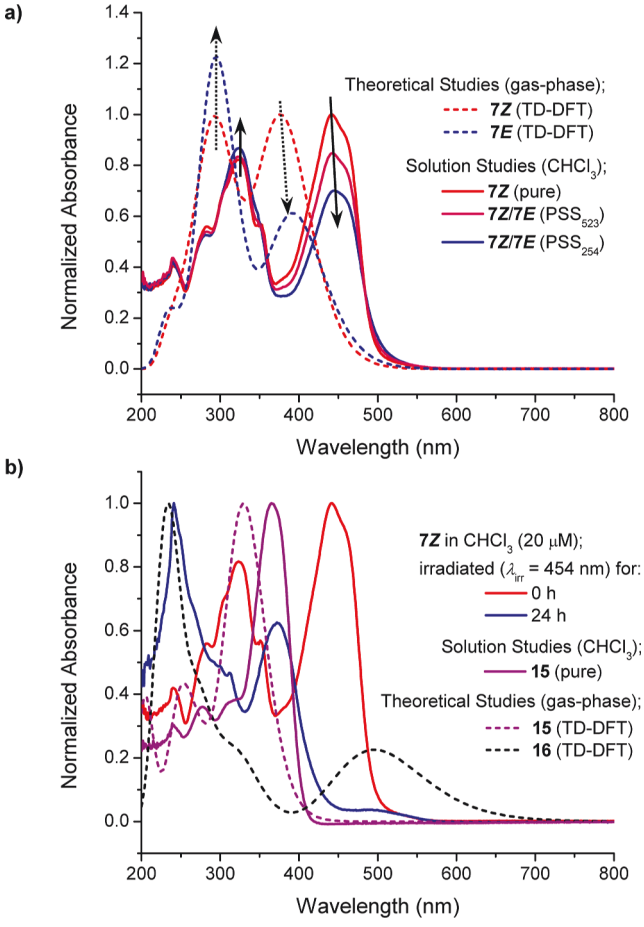

Figure 9. (a) Experimental absorption spectra (solid line) of pure 7*Z* (red) and upon irradiation with different light sources (λ_{irr} = 254 and 523 nm) in solution and time-dependent DFT predicted UV−vis spectra (dashed lines) of 7*Z* (red) and 7*E* (blue). (b) UV−vis evidence of photoinduced tandem pericyclic reactions for 7*Z* in solution (solid lines) under prolonged exposure to 454 nm light and time-dependent DFT predicted UV−vis spectra (dashed lines) for compound **15** (purple) and **16** (black).

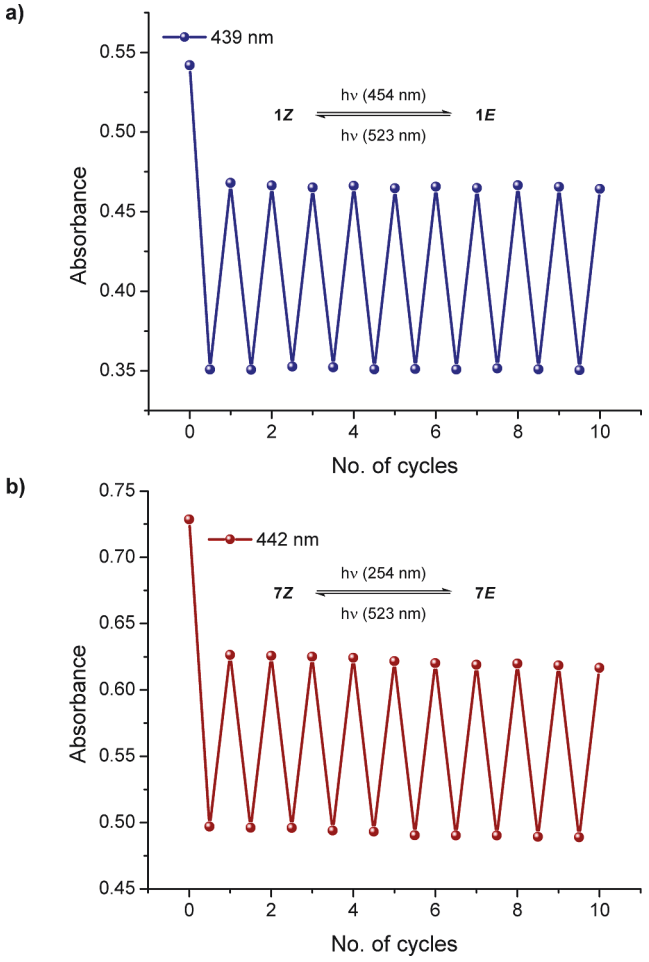

Figure 10. (a) Photoswitching of compound **1** (chloroform, 20 μM). The absorbance change at λ_{max} = 439 nm was monitored while alternating between 454 and 523 nm wavelengths of irradiation. (b) Photoswitching of compound **7** (chloroform, 20 μM). The absorbance change at λ_{max} = 442 nm was monitored while alternating between 254 and 523 nm wavelengths of irradiation.

it was restricted to 454 nm irradiation. We used ground-state *Z*/*E* configurational energies and conformational preferences obtained from DFT calculations to shed light on the disparate behavior. The DFT predicted optimized geometries of the target molecules in their lowest energy conformers and the frontier molecular orbitals are shown in Figures S41−S57 and Table S3. The energy values for the target molecules are given in Table 2. For target molecule **1**, the lowest energy conformer in the *Z* configuration is s-*cis*, adopting a planar geometry (Figure 4d,e) that matches quite well with the XRD analysis. To confirm the lowest energy conformer of distorted **1***E*, a

https://doi.org/10.1021/acs.chemmater.3c01607
Chem. Mater. 2023, 35, 8122−8134

rigid scan was performed by calculating single point energies along the torsional angle between C8−C12−C13−S1 through 360° rotation to generate a potential energy surface (Figure S39). The lowest energy conformer has a dihedral angle of 90° defined by C8−C12−C13−S1, which upon further optimization presents the s-*trans* conformation as the most stable conformer (Figure S39). For compound **1**, the s-*trans* (6.14 kcal/mol) conformer in the *E* state is about 0.47 kcal/mol lower in energy than the s-*cis* conformer (6.61 kcal/mol) in the same *E* configuration (Figure S40 and Table S4).

Similarly, the s-*cis* conformer of **7***Z* is found to be the most stable, whereas the s-*trans* conformer of **7***E* is found to be lower in energy than the s-*cis* conformer in the *E* configuration. The results suggest that the higher population will tend to adopt the s-*trans* conformation over s-*cis* owing to photoirradiation. The data clarifies the role of photoisomerization in the tandem pericyclic reactions, since only in the s-*trans* conformation are the molecular orbitals aligned to promote a symmetry allowed six electron electrocyclization. This theoretical study clarifies the observation of minor and major degradation for molecules **1**, **2**, **4**, and **7** respectively, for which the s-*trans* conformer is more stable than the s-*cis* one. The different photochemical behavior of these molecules upon irradiation with different sources of excitation might be attributed to the fact that 454 nm LED light could promote a higher population of **7***E* isomers to the s-*trans* conformer compared to the s-*cis*, as opposed to other irradiation sources as they absorb most strongly at this wavelength.

Interestingly, the optimized geometries of **3***E* and **8***E* reveal the s-*trans* conformer as higher in energy than s-*cis* due to steric interactions between the dicyanomethylene moiety and the alkyl chain attached to the thiophene ring (Figure S40). Consequently, no degradation is observed for **3** and **8**, even under 454 nm irradiation, since the s-*cis* conformer of the *E* isomer does not meet the geometric requirements for the electrocyclic reaction. The importance of the regiochemistry of the alkyl chain can also be explained by comparing molecules **2** and **3**. For **2***E*, the s-*trans* conformation is more stable than s-*cis*, as the alkyl chain is pointed away from the INCN unit in both, unlike **3***E*. Consequently, molecule **2** undergoes minor degradation with 454 nm light, while **3** shows well-behaved isomerization. Although the alkyl chain plays a significant role in the photodegradation behavior, it does not provide any conclusive role on *the extent of* photoisomerization of these molecules, contrary to the previous literature.[34] The evidence shows that molecule **3**, having an alkyl chain pointing toward the INCN unit, unlike **1** and **2**, can nonetheless yield a higher percentage of *E* isomer at the PSS upon irradiation with 454 and 523 nm light (versus molecules **1** and **2**). Similarly, molecules **7** and **8** undergo photoisomerization to an extent similar to those at these irradiation sources. Hence, conformational preferences are likely contributing factors to the disparate photochemical behavior of the INCN-functionalized small molecules.

Thermal Relaxation Studies. Thermal **1***E* → **1***Z* isomerization in solution (15 mM, chloroform-*d*) could be observed by keeping a PSS mixture of **1***Z*/**1***E* in the dark. After 24 h at room temperature, the **1***Z*/**1***E* composition is 59/41, differing from the 51/49 PSS composition (Figure S18), confirming the thermodynamic preference for **1***Z*. For a detailed investigation of **1***E* → **1***Z* isomerization, further experiments were performed at elevated temperature (70 °C) with ^{1}H NMR monitoring. In toluene-d_8, upon 254 nm irradiation, the **1***Z*/**1***E* PSS composition is 48/52. Upon thermal treatment of the postirradiation sample for 1 h (at 70 °C), the PSS ratio changes to 51/49 (Figures S19 and S20). In tetrachloroethane-d_2, 254 nm irradiation results in a 60/40 **1***Z*/**1***E* ratio, and upon thermal treatment for 1 h (at 70 °C), the composition changes to 75/25 (Figures S21 and S22). However, in acetonitrile-d_3, 254 nm irradiation results in a 50/50 **1***Z*/**1***E* PSS mixture, and upon thermal treatment (at 70 °C), complete conversion to the *Z* isomer is observed within 19 min of irradiation (Figures S23 and S24). So, the change observed in the **1***E* isomer composition is 6% in toluene-d_8 upon 1 h of thermal treatment, 38% in tetrachloroethane-d_2, and 100% in acetonitrile-d_3. The thermal relaxation studies in different polarity solvents suggest that the process might be faster in more polar solvents (e.g., acetonitrile) versus less polar ones (e.g., tetrachloroethane and toluene). These qualitative studies will be supported by detailed quantitative studies to determine kinetic parameters in the future.

CONCLUSIONS

We have synthesized eight INCN-functionalized π-conjugated molecules and demonstrated their well-controlled photochemical behavior upon excitation at selective wavelengths of 254, 371, 454, and 523 nm. Stereochemical analysis of model compounds **1**−**8** has shown that the thermodynamically preferred *Z* isomers are the only detectable isomers obtained from synthesis, with the corresponding *E* forms obtained from selective irradiation and *Z*/*E* photoisomerization in solution. One exception is **7***Z*, which following *Z*/*E* photoisomerization with 454 nm irradiation undergoes a tandem electrocyclization and sigmatropic rearrangement reaction. The results comport with the findings of Perepichka and co-workers in their studies of the popular nonfullerene acceptor, IT-4F.[33] Complementary ground- and excited-state DFT studies have highlighted the significance of the configurational (i.e., *Z* or *E*) and conformational (i.e., s-*cis* or s-*trans*) preferences on the photochemical behavior. The facile and fatigue-resistant photoswitching observed for the INCN family demonstrates good photostability and the potential for photoswitch development. Overall, this structure−property relationship study demonstrates the well-controlled photochemical behavior of INCN-functionalized π-systems and will hopefully encourage the design of new stimuli-responsive functional organic materials.

EXPERIMENTAL METHODS

Materials. Reagents and solvents were purchased from commercial sources and used without further purification, unless otherwise specified. THF was degassed in a 20 L drum and passed through activated alumina under a positive argon atmosphere. Thin layer chromatography (TLC) was performed on SiO_2-60 F_{254} aluminum plates with visualization by UV light. Column chromatography was performed using silica gel technical grade, pore size 60 Å, 230−400 mesh particle size, 40−63 μm particle size from Sigma-Aldrich.

Note: Due to the photosensitivity of the INCN-functionalized products, the reaction vessels were covered with aluminum foil during the synthesis of **1***Z*−**8***Z*. To minimize unintentional photoisomerization, aluminum foil was used to cover all glassware during purification processes such that any source of excessive light exposure was eliminated, while samples were dissolved in solution.

Photoisomerization Techniques. The photoisomerization studies were performed using selective irradiation sources of 254, 371, 454, 523, and 628 nm. Ultraviolet irradiations were achieved using an LSE Lighting (Model no. CFL15/UV/MED) compact

https://doi.org/10.1021/acs.chemmater.3c01607
Chem. Mater. 2023, 35, 8122−8134

fluorescent light bulb (15 W, 120 V) emitting a peak irradiation wavelength of 254 nm and a UV lamp (36 W) irradiating at 371 nm. Due to the heat given off from the UV bulbs, a cooling fan was used for all irradiation experiments requiring UV irradiation, resulting in a measured temperature at the hottest point near the bulb of 28 °C. Blue LED irradiation was achieved using a Westinghouse Lighting (model no. 3315100) 100-W Equivalent PAR38 Flood Blue Outdoor Weatherproof LED Light Bulb (15 W, 120 V) emitting a peak irradiation wavelength of 454 nm. Green LED irradiation was achieved using a Westinghouse Lighting (model no. 3314900) 100-W Equivalent PAR38 Flood Green Outdoor Weatherproof LED Light Bulb (15 W, 120 V) emitting a peak irradiation wavelength of 523 nm. Red LED irradiation was achieved using Westinghouse Lighting (model no. 3314700) 100 W Equivalent PAR38 Flood Green Outdoor Weatherproof LED Light Bulb (15 W, 120 V) emitting a peak irradiation wavelength of 628 nm. No cooling fan was required for the LED irradiation sources.

NMR Techniques. ^{1}H NMR spectra were recorded on an INOVA-500 (500 MHz) and Bruker 600 MHz spectrometer and ^{13}C and ^{19}F were recorded on a Bruker 600 MHz spectrometer (^{13}C at 151 MHz and ^{19}F at 565 MHz). Chemical shifts (δ) are given in parts per million (ppm) referenced to residual deuterated solvent purchased from Cambridge Isotope Laboratories, Inc. ($CDCl_3$: δ H 7.26 ppm, δ C 77.16 ppm). Abbreviations used are s (singlet), d (doublet), t (triplet), q (quartet), and m (multiplet). All of the photoirradiation experiments using ^{1}H NMR spectroscopy were performed on an INOVA-500 (^{1}H at 500 MHz) spectrometer. To determine the photostationary state composition of each INCN-functionalized target molecule, a 15 mM stock solution (5 mM for molecule **4***Z* due to its poor solubility) in chloroform-*d* was prepared, and approximately 0.5 mL of the stock solution was placed in a conventional glass NMR tube unless otherwise specified. The samples were exposed to an appropriate irradiation wavelength. The integral ratios of signals corresponding to the *Z* isomer and the *E* isomer were compared to calculate the relative percentage of each species in solution. The samples were irradiated, and ^{1}H NMR spectra were recorded until changes in the *Z*/*E* integral ratios were no longer observed, indicating that the photostationary state had been reached. All of these experiments were performed using aerated solutions of compounds **1***Z*−**8***Z*.

UV−Vis Spectroscopy. Solution absorption spectra were measured for the compounds in chloroform on a PerkinElmer Lambda 25 dual beam absorption spectrometer and a Cary 100 Bio spectrophotometer using 1 cm quartz cells. Spectrophotometric grade solvents were used for the absorption studies. Solutions of **1***Z*−**8***Z* (3.0 mL) in chloroform were prepared and transferred into a quartz cuvette for immediate UV/vis absorption measurements. Conducting the photoirradiation experiment using UV−vis, significant photodegradation was observed in solution (20 μM, chloroform) using a quartz cuvette at 254 nm irradiation with the difference between NMR and UV−vis irradiation conditions being the medium of the solution container (glass versus quartz). Hence, the cuvettes were removed from the spectrophotometer and covered with a glass container while irradiated at an appropriate wavelength of excitation (λ_{irr} = 254, 454, 523 nm) and absorption spectra were recorded to monitor the changes in the UV−vis spectrum attributed to the isomerization process. The samples were irradiated until no changes in the UV−vis spectra were observed, indicating that the respective photostationary states (PSS) were reached. All these experiments were performed using aerated solutions of compounds **1***Z*−**8***Z*.

Theoretical Calculations. Ground state geometries and conformational analyses were conducted in the gas phase at the B3LYP/6-31+G(d) level as implemented in Gaussian 09.[48] All octyl chains were truncated to methyl groups to reduce computational cost. Excited state calculations were performed at the CAM-B3LYP/cc-pVDZ level of theory by using the coordinates from the previously optimized geometries. Molecular orbital plots were made using VMD[49] from the Gaussian output files or using the Avogadro visualization software.[50] Frontier molecular orbital shapes were visualized using the Avogadro molecular editor and visualization software.

■ ASSOCIATED CONTENT

Supporting Information

The Supporting Information is available free of charge at https://pubs.acs.org/doi/10.1021/acs.chemmater.3c01607.

Synthesis schemes; written characterization data; ^{1}H NMR spectra; ^{13}C NMR spectra; ^{19}F NMR spectra (^{1}H coupled); ^{19}F NMR spectra (^{1}H decoupled); 2D NMR characterization; irradiation sources; thin-layer chromatography; NMR photoisomerization studies; NMR thermal isomerization studies; UV-VIS isomerization studies; UV-VIS photoswitching studies; computational details; and X-ray crystallography (PDF)

■ AUTHOR INFORMATION

Corresponding Author

Ronald K. Castellano − *Department of Chemistry, University of Florida, Gainesville, Florida 32611, United States;* orcid.org/0000-0003-4322-9932; Email: castellano@chem.ufl.edu

Authors

Parag Das − *Department of Chemistry, University of Florida, Gainesville, Florida 32611, United States*

Cory T. Kornman − *Department of Chemistry, University of Florida, Gainesville, Florida 32611, United States*

Ion Ghiviriga − *Department of Chemistry, University of Florida, Gainesville, Florida 32611, United States;* orcid.org/0000-0001-5812-5170

Khalil A. Abboud − *Department of Chemistry, University of Florida, Gainesville, Florida 32611, United States*

Complete contact information is available at: https://pubs.acs.org/10.1021/acs.chemmater.3c01607

Notes

The authors declare no competing financial interest.

■ ACKNOWLEDGMENTS

Acknowledgment is made to National Science Foundation for funding support of this research (CHE-1904534). C.T.K. wishes to acknowledge the University of Florida (UF) Department of Chemistry for providing a Graduate School Fellowship (GSF) that made this research possible. We acknowledge the University of Florida Research Computing for providing computational resources and support that have contributed to the research results reported in this publication (https://www.rc.ufl.edu). The mass spectrometric data were obtained by the UF Department of Chemistry Mass Spectrometry Research and Education Center supported, in part, by the National Institutes of Health (S10OD021758-01A1). We would like to thank the UF Center for Nuclear Magnetic Resonance Spectroscopy for providing equipment and support that have contributed to these published results. We would also like to thank Prof. Jiangeng Xue, Dr. David Camero, and Nathan Grinalds for their insightful conversations and help with recording the emission profiles of the selective irradiation sources used in this work.

REFERENCES

(1) Schweda, B.; Reinfelds, M.; Hofstadler, P.; Trimmel, G.; Rath, T. Recent Progress in the Design of Fused-Ring Non-Fullerene Acceptors−Relations between Molecular Structure and Optical, Electronic, and Photovoltaic Properties. *ACS Appl. Energy Mater.* **2021**, *4* (11), 11899−11981.

(2) Huang, J.; Tang, H.; Yan, C.; Li, G. 1,1-Dicyanomethylene-3-Indanone End-Cap Engineering for Fused-Ring Electron Acceptor-Based High-Performance Organic Photovoltaics. *Cell Rep. Phys. Sci.* **2021**, *2* (1), 100292.

(3) Lin, Y.; Wang, J.; Zhang, Z.-G.; Bai, H.; Li, Y.; Zhu, D.; Zhan, X. An Electron Acceptor Challenging Fullerenes for Efficient Polymer Solar Cells. *Adv. Mater.* **2015**, *27* (7), 1170−1174.

(4) Zhao, W.; Li, S.; Yao, H.; Zhang, S.; Zhang, Y.; Yang, B.; Hou, J. Molecular Optimization Enables over 13% Efficiency in Organic Solar Cells. *J. Am. Chem. Soc.* **2017**, *139* (21), 7148−7151.

(5) Zhang, H.; Yao, H.; Hou, J.; Zhu, J.; Zhang, J.; Li, W.; Yu, R.; Gao, B.; Zhang, S.; Hou, J. Over 14% Efficiency in Organic Solar Cells Enabled by Chlorinated Nonfullerene Small-Molecule Acceptors. *Adv. Mater.* **2018**, *30* (28), 1800613.

(6) Hou, J.; Inganäs, O.; Friend, R. H.; Gao, F. Organic solar cells based on non-fullerene acceptors. *Nat. Mater.* **2018**, *17* (2), 119−128.

(7) Heumueller, T.; Mateker, W. R.; Distler, A.; Fritze, U. F.; Cheacharoen, R.; Nguyen, W. H.; Biele, M.; Salvador, M.; von Delius, M.; Egelhaaf, H.-J.; McGehee, M. D.; Brabec, C. J. Morphological and electrical control of fullerene dimerization determines organic photovoltaic stability. *Energy Environ. Sci.* **2016**, *9* (1), 247−256.

(8) Armin, A.; Li, W.; Sandberg, O. J.; Xiao, Z.; Ding, L.; Nelson, J.; Neher, D.; Vandewal, K.; Shoaee, S.; Wang, T.; Ade, H.; Heumüller, T.; Brabec, C.; Meredith, P. A History and Perspective of Non-Fullerene Electron Acceptors for Organic Solar Cells. *Adv. Energy Mater.* **2021**, *11* (15), 2003570.

(9) Yuan, J.; Zhang, Y.; Zhou, L.; Zhang, G.; Yip, H.-L.; Lau, T.-K.; Lu, X.; Zhu, C.; Peng, H.; Johnson, P. A.; Leclerc, M.; Cao, Y.; Ulanski, J.; Li, Y.; Zou, Y. Single-Junction Organic Solar Cell with over 15% Efficiency Using Fused-Ring Acceptor with Electron-Deficient Core. *Joule* **2019**, *3* (4), 1140−1151.

(10) Zhang, M.; Zhu, L.; Zhou, G.; Hao, T.; Qiu, C.; Zhao, Z.; Hu, Q.; Larson, B. W.; Zhu, H.; Ma, Z.; Tang, Z.; Feng, W.; Zhang, Y.; Russell, T. P.; Liu, F. Single-layered organic photovoltaics with double cascading charge transport pathways: 18% efficiencies. *Nat. Commun.* **2021**, *12* (1), 309.

(11) Zhao, F.; Dai, S.; Wu, Y.; Zhang, Q.; Wang, J.; Jiang, L.; Ling, Q.; Wei, Z.; Ma, W.; You, W.; Wang, C.; Zhan, X. Single-Junction Binary-Blend Nonfullerene Polymer Solar Cells with 12.1% Efficiency. *Adv. Mater.* **2017**, *29* (18), 1700144.

(12) Ke, X.; Meng, L.; Wan, X.; Li, M.; Sun, Y.; Guo, Z.; Wu, S.; Zhang, H.; Li, C.; Chen, Y. The rational and effective design of nonfullerene acceptors guided by a semi-empirical model for an organic solar cell with an efficiency over 15%. *J. Mater. Chem. A* **2020**, *8* (19), 9726−9732.

(13) Meng, L.; Zhang, Y.; Wan, X.; Li, C.; Zhang, X.; Wang, Y.; Ke, X.; Xiao, Z.; Ding, L.; Xia, R.; Yip, H.; Cao, Y.; Chen, Y. Organic and solution-processed tandem solar cells with 17.3% efficiency. *Science* **2018**, *361* (6407), 1094−1098.

(14) Liu, F.; Zhou, L.; Liu, W.; Zhou, Z.; Yue, Q.; Zheng, W.; Sun, R.; Liu, W.; Xu, S.; Fan, H.; Feng, L.; Yi, Y.; Zhang, W.; Zhu, X. Organic Solar Cells with 18% Efficiency Enabled by an Alloy Acceptor: A Two-in-One Strategy. *Adv. Mater.* **2021**, *33* (27), 2100830.

(15) Liu, Q.; Jiang, Y.; Jin, K.; Qin, J.; Xu, J.; Li, W.; Xiong, J.; Liu, J.; Xiao, Z.; Sun, K.; Yang, S.; Zhang, X.; Ding, L. 18% Efficiency organic solar cells. *Sci. Bull.* **2020**, *65* (4), 272−275.

(16) Zhao, F.; Wang, C.; Zhan, X. Morphology Control in Organic Solar Cells. *Adv. Energy Mater.* **2018**, *8* (28), 1703147.

(17) Dou, L.; Liu, Y.; Hong, Z.; Li, G.; Yang, Y. Low-Bandgap Near-IR Conjugated Polymers/Molecules for Organic Electronics. *Chem. Rev.* **2015**, *115* (23), 12633−12665.

(18) Du, Z.; Chen, W.; Chen, Y.; Qiao, S.; Bao, X.; Wen, S.; Sun, M.; Han, L.; Yang, R. High efficiency solution-processed two-dimensional small molecule organic solar cells obtained via low-temperature thermal annealing. *J. Mater. Chem. A* **2014**, *2* (38), 15904−15911.

(19) Grand, C.; Zajaczkowski, W.; Deb, N.; Lo, C. K.; Hernandez, J. L.; Bucknall, D. G.; Müllen, K.; Pisula, W.; Reynolds, J. R. Morphology Control in Films of Isoindigo Polymers by Side-Chain and Molecular Weight Effects. *ACS Appl. Mater. Interfaces* **2017**, *9* (15), 13357−13368.

(20) Zhang, Q.; Kan, B.; Liu, F.; Long, G.; Wan, X.; Chen, X.; Zuo, Y.; Ni, W.; Zhang, H.; Li, M.; Hu, Z.; Huang, F.; Cao, Y.; Liang, Z.; Zhang, M.; Russell, T. P.; Chen, Y. Small-molecule solar cells with efficiency over 9%. *Nat. Photonics* **2015**, *9* (1), 35−41.

(21) Kan, B.; Li, M.; Zhang, Q.; Liu, F.; Wan, X.; Wang, Y.; Ni, W.; Long, G.; Yang, X.; Feng, H.; Zuo, Y.; Zhang, M.; Huang, F.; Cao, Y.; Russell, T. P.; Chen, Y. A Series of Simple Oligomer-like Small Molecules Based on Oligothiophenes for Solution-Processed Solar Cells with High Efficiency. *J. Am. Chem. Soc.* **2015**, *137* (11), 3886−3893.

(22) Zuo, Y.; Zhang, Q.; Wan, X.; Li, M.; Zhang, H.; Li, C.; Chen, Y. A small molecule with selenophene as the central block for high performance solution-processed organic solar cells. *Org. Electron.* **2015**, *19*, 98−104.

(23) Kan, B.; Zhang, Q.; Wan, X.; Ke, X.; Wang, Y.; Feng, H.; Zhang, M.; Chen, Y. Oligothiophene-based small molecules with 3,3′-difluoro-2,2′-bithiophene central unit for solution-processed organic solar cells. *Org. Electron.* **2016**, *38*, 172−179.

(24) Camero, D. M.; Grinalds, N. J.; Kornman, C. T.; Barba, S.; Li, L.; Weldeab, A. O.; Castellano, R. K.; Xue, J. Thin-Film Morphology and Optical Properties of Photoisomerizable Donor-Acceptor Oligothiophenes. *ACS Appl. Mater. Interfaces* **2023**, *15* (21), 25134−25147.

(25) Yang, Y.; Zhang, Z.-G.; Bin, H.; Chen, S.; Gao, L.; Xue, L.; Yang, C.; Li, Y. Side-Chain Isomerization on an n-type Organic Semiconductor ITIC Acceptor Makes 11.77% High Efficiency Polymer Solar Cells. *J. Am. Chem. Soc.* **2016**, *138* (45), 15011−15018.

(26) Ryu, H. S.; Kim, M. J.; Lee, Y. W.; Lee, S.-H.; Shin, T. J.; Cho, J. H.; Woo, H. Y. Synthesis, Molecular Packing, and Electrical Properties of New Regioisomeric n-type Semiconducting Molecules with Modification of Alkyl Substituents Position. *ACS Appl. Mater. Interfaces* **2019**, *11* (50), 47170−47181.

(27) Lai, H.; Chen, H.; Zhou, J.; Qu, J.; Chao, P.; Liu, T.; Chang, X.; Zheng, N.; Xie, Z.; He, F. Isomer-free: Precise Positioning of Chlorine-Induced Interpenetrating Charge Transfer for Elevated Solar Conversion. *iScience* **2019**, *17*, 302−314.

(28) Li, T.; Wu, Y.; Zhou, J.; Li, M.; Wu, J.; Hu, Q.; Jia, B.; Pan, X.; Zhang, M.; Tang, Z.; Xie, Z.; Russell, T. P.; Zhan, X. Butterfly Effects Arising from Starting Materials in Fused-Ring Electron Acceptors. *J. Am. Chem. Soc.* **2020**, *142* (47), 20124−20133.

(29) Kornman, C. T.; Li, L.; Weldeab, A. O.; Ghiviriga, I.; Abboud, K. A.; Castellano, R. K. Photoisomerization of dicyanorhodanine-functionalized thiophenes. *Chem. Sci.* **2020**, *11* (37), 10190−10197.

(30) Guo, W.; Zhao, B.; Xin, J.; Liu, H.; Mi, Y.; Zhang, J.; Guo, Z.; Wei, W.; Ma, W.; Gao, C.; An, Z. Non-fullerene small molecular acceptors based on dithienocyclopentafluorene and dithienocyclopentacarbazole cores for polymer solar cells. *Dyes Pigm.* **2017**, *144*, 48−57.

(31) Wu, Z.; Qiu, R.; Jiang, H.; Wang, Q.; Chen, Y.; Liu, H.; Xie, S.; Yip, H.-L.; Zhang, L.; Chen, J. Synthesis and photovoltaic performance of a non-fullerene acceptor comprising siloxane-terminated alkoxyl side chain. *Org. Electron.* **2021**, *91*, 106087.

(32) Ren, L.; Liang, L.; Zhang, Z.; Zhang, Z.; Xiong, Q.; Zhao, N.; Yu, Y.; Scopelliti, R.; Gao, P. The roles of fused-ring organic semiconductor treatment on SnO2 in enhancing perovskite solar cell performance. *RSC Adv.* **2021**, *11* (7), 3792−3800.

(33) Che, Y.; Niazi, M. R.; Izquierdo, R.; Perepichka, D. F. Mechanism of the Photodegradation of A-D-A Acceptors for Organic Photovoltaics**. *Angew. Chem., Int. Ed.* **2021**, *60* (47), 24833−24837.

https://doi.org/10.1021/acs.chemmater.3c01607
Chem. Mater. 2023, 35, 8122−8134

(34) Liu, Z.-X.; Yu, Z.-P.; Shen, Z.; He, C.; Lau, T.-K.; Chen, Z.; Zhu, H.; Lu, X.; Xie, Z.; Chen, H.; Li, C.-Z. Molecular insights of exceptionally photostable electron acceptors for organic photovoltaics. *Nat. Commun.* **2021**, *12* (1), 3049.
(35) Che, Y.; Niazi, M. R.; Chan, Q.; Ghamari, P.; Yu, T.; Ruchlin, C.; Yu, H.; Yan, H.; Ma, D.; Xiao, S. S.; Izquierdo, R.; Perepichka, D. F. Design of Furan-Based Acceptors for Organic Photovoltaics. *Angew. Chem., Int. Ed.* **2023**, No. e202309003.
(36) Boelke, J.; Hecht, S. Designing Molecular Photoswitches for Soft Materials Applications. *Adv. Opt. Mater.* **2019**, *7* (16), 1900404.
(37) Goulet-Hanssens, A.; Eisenreich, F.; Hecht, S. Enlightening Materials with Photoswitches. *Adv. Mater.* **2020**, *32* (20), 1905966.
(38) Kobauri, P.; Dekker, F. J.; Szymanski, W.; Feringa, B. L. Rational Design in Photopharmacology with Molecular Photoswitches. *Angew. Chem., Int. Ed.* **2023**, *62* (30), No. e202300681.
(39) Elvidge, C. D.; Keith, D. M.; Tuttle, B. T.; Baugh, K. E. Spectral Identification of Lighting Type and Character. *Sensors* **2010**, *10*, 3961−3988.
(40) Waldeck, D. H. Photoisomerization dynamics of stilbenes. *Chem. Rev.* **1991**, *91* (3), 415−436.
(41) Bandara, H. M. D.; Burdette, S. C. Photoisomerization in different classes of azobenzene. *Chem. Soc. Rev.* **2012**, *41* (5), 1809−1825.
(42) Wiedbrauk, S.; Dube, H. Hemithioindigo—an emerging photoswitch. *Tetrahedron Lett.* **2015**, *56* (29), 4266−4274.
(43) Li, G.; Zhang, X.; Jones, L. O.; Alzola, J. M.; Mukherjee, S.; Feng, L.-w.; Zhu, W.; Stern, C. L.; Huang, W.; Yu, J.; Sangwan, V. K.; DeLongchamp, D. M.; Kohlstedt, K. L.; Wasielewski, M. R.; Hersam, M. C.; Schatz, G. C.; Facchetti, A.; Marks, T. J. Systematic Merging of Nonfullerene Acceptor π-Extension and Tetrafluorination Strategies Affords Polymer Solar Cells with > 16% Efficiency. *J. Am. Chem. Soc.* **2021**, *143* (16), 6123−6139.
(44) Aldrich, T. J.; Matta, M.; Zhu, W.; Swick, S. M.; Stern, C. L.; Schatz, G. C.; Facchetti, A.; Melkonyan, F. S.; Marks, T. J. Fluorination Effects on Indacenodithienothiophene Acceptor Packing and Electronic Structure, End-Group Redistribution, and Solar Cell Photovoltaic Response. *J. Am. Chem. Soc.* **2019**, *141* (7), 3274−3287.
(45) Norton Matos, M. R. P.; Gois, P. M. P.; Mata, M. L. E. N.; Cabrita, E. J.; Afonso, C. A. M. Studies on the Preparation of 4-Ethoxyalkyliden and 4-Aminoalkyliden-5(4H)-oxazolones. *Synth. Commun.* **2003**, *33* (8), 1285−1299.
(46) Jacquemin, D.; Planchat, A.; Adamo, C.; Mennucci, B. TD-DFT Assessment of Functionals for Optical 0−0 Transitions in Solvated Dyes. *J. Chem. Theory Comput.* **2012**, *8* (7), 2359−2372.
(47) Ali, A.; Rafiq, M. I.; Zhang, Z.; Cao, J.; Geng, R.; Zhou, B.; Tang, W. TD-DFT benchmark for UV-visible spectra of fused-ring electron acceptors using global and range-separated hybrids. *Phys. Chem. Chem. Phys.* **2020**, *22* (15), 7864−7874.
(48) Frisch, M. J.; Trucks, G. W.; Schlegel, H. B.; Scuseria, G. E.; Robb, M. A.; Cheeseman, J. R.; Scalmani, G.; Barone, V.; Mennucci, B.; Petersson, G. A.; Nakatsuji, H.; Caricato, M.; Li, X.; Hratchian, H. P.; Izmaylov, A. F.; Bloino, J.; Zheng, G.; Sonnenberg, J. L.; Hada, M.; Ehara, M.; Toyota, K.; Fukuda, R.; Hasegawa, J.; Ishida, M.; Nakajima, T.; Honda, Y.; Kitao, O.; Nakai, H.; Vreven, T.; Montgomery, J. A.; Peralta, J. E.; Ogliaro, F.; Bearpark, M.; Heyd, J. J.; Brothers, E.; Kudin, K. N.; Staroverov, V. N.; Keith, T.; Kobayashi, R.; Normand, J.; Raghavachari, K.; Rendell, A.; Burant, J. C.; Iyengar, S. S.; Tomasi, J.; Cossi, M.; Rega, N.; Millam, J. M.; Klene, M.; Knox, J. E.; Cross, J. B.; Bakken, V.; Adamo, C.; Jaramillo, J.; Gomperts, R.; Stratmann, R. E.; Yazyev, O.; Austin, A. J.; Cammi, R.; Pomelli, C.; Ochterski, J. W.; Martin, R. L.; Morokuma, K.; Zakrzewski, V. G.; Voth, G. A.; Salvador, P.; Dannenberg, J. J.; Dapprich, S.; Daniels, A. D.; Farkas, O.; Foresman, J. B.; Ortiz, J. V.; Cioslowski, J.; Fox, D. J. *Gaussian 09*. Revision D.01; Gaussian, Inc.: Wallingford, CT, 2013;.Jr
(49) Humphrey, W.; Dalke, A.; Schulten, K. VMD: Visual molecular dynamics. *J. Mol. Graph.* **1996**, *14* (1), 33−38.
(50) Hanwell, M. D.; Curtis, D. E.; Lonie, D. C.; Vandermeersch, T.; Zurek, E.; Hutchison, G. R. Avogadro: an advanced semantic chemical editor, visualization, and analysis platform. *J. Cheminf.* **2012**, *4* (1), 17.

https://doi.org/10.1021/acs.chemmater.3c01607
Chem. Mater. 2023, 35, 8122−8134